Macromolecules

pubs.acs.org/Macromolecules
Article

Dynamics of Syndiotactic Polypropylene

Michaela Zamponi,* Wim Pyckhout-Hintzen, Andreas Wischnewski, Vitaliy Pipich, Olaf Holderer, Bela Farago, Geoffrey W. Coates, Brian K. Long, Michael Monkenbusch, and Dieter Richter

Cite This: *Macromolecules* 2024, 57, 3098−3108

ABSTRACT: We present a study of the structure and dynamics of long-chain syndiotactic polypropylene (s-PP) melts by small-angle neutron scattering (SANS), rheology, neutron backscattering, and neutron spin echo spectroscopy (NSE). From SANS, we determine the characteristic ratio of C_∞ = 11.5, which is larger than that obtained from previous experiments but in good agreement with simulation. Concerning dynamics, in the Rouse regime, neutron backscattering and incoherent NSE revealed Rouse rates that very well agree with each other, demonstrating the consistency of measurements in energy and time space. The single-chain dynamic structure factor was also measured by NSE. As none of the conventional data evaluation schemes for local reptation were successfully applicable, we used the novel extended de Gennes dynamic structure factor [Monkenbusch, M. et al. *J. Chem. Phys.* **2023**, *159*, 034902]. We found that s-PP displays a strongly asymmetric tube with an aspect ratio of about 0.5. Allowing for a small non-Gaussianity improves the fit. The scaling properties of the Monkenbusch dynamic structure factor are well fulfilled also for s-PP. Contrary to intuition, the tube asymmetry appears not to be related to chain stiffness at least not in the range of C_∞ = 5 (polyisoprene) and 11.5 (s-PP).

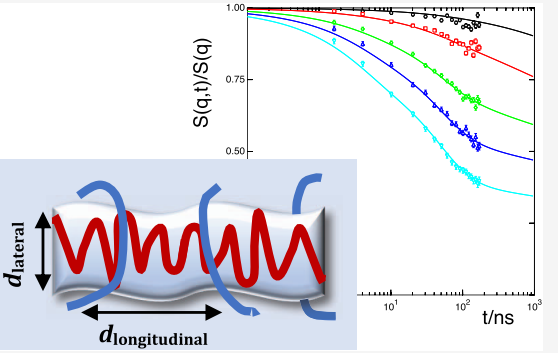

I. INTRODUCTION

Long-chain polymer melts exhibit a salient viscoelastic behavior. The rheological properties stem from topological confinements: in the melt, the long polymer chains entangle each other and mutually restrict their lateral segmental motions. A given chain is then confined to motion along its own contour. The most successful model to describe this entangled dynamics is the reptation model,[1−3] which describes the lateral constraints by a virtual tube. At early times within the tube, the long chains undergo free Rouse motion[4] as is the case for short unentangled chains. When the chains start to feel the constraints by the others, the motion then can only occur along a tube-like profile, and the chains "reptate". The lateral confinement length, which may be described as a tube diameter, is thereby identified as the distance between two entanglements along the chain, which corresponds to the step length of the tube. The introduction of only one additional parameter, the tube diameter, is already sufficient to describe the entangled polymer dynamics.

However, the existence of only one confinement length in long-chain polymer melts as assumed in the reptation model has been questioned by mechanical (rheology) and microscopic measurements (neutron spin echo spectroscopy (NSE)) on polyethylene (PE) and poly(ethylene-propylene) (PEP),[5] as well as poly(ethylene oxide) (PEO),[6] which yielded different values for the tube diameter. In the theory of viscoelasticity, the plateau modulus obtained by rheological measurements is related to the microscopic tube diameter, which can be determined by NSE investigations. NSE spectroscopy on a few protonated chains in a deuterated matrix observes the segmental fluctuations of the chain. For the different polymers, the value of the tube diameter obtained by NSE is higher than the rheological value; however, the ratio d_{rheo}/d_{NSE} is about the same. This points to a general feature that could be explained by the different measuring methods. If this were true and there would exist only one length scale, their ratio should be comparable for all polymers.

In a recent paper,[7] the dynamic data of 5 different polymers have been revisited and reanalyzed. As before, they observed different tube diameters as determined from rheology and NSE, albeit with a similar ratio between NSE and rheology results. To analyze the NSE data more thoroughly, the standard tube model has been extended to incorporate the Rouse dynamics within the tube and non-Gaussianity effects. Moreover, a tentative asymmetry factor was introduced to allow for a difference in lateral and longitudinal tube dimensions. For the different polymers, there seems to be an indication of an asymmetric tube, although the asymmetry factor is relatively close to 1 except for the case of polyisoprene

Received: December 14, 2023
Revised: February 13, 2024
Accepted: March 5, 2024
Published: March 19, 2024

https://doi.org/10.1021/acs.macromol.3c02529
Macromolecules 2024, 57, 3098−3108

(PI). From MD simulations of PE and polybutadiene (PB),[8] some larger differences in lateral and longitudinal tube dimensions were found, with the ratio varying between 0.7 and 0.9.

To rule out the possibility that the systematic difference in the tube diameter from NSE and rheology is just due to different measuring and interpretation methods and to further explore the anisotropic confinement in the NSE data, a polymer with different properties has to be investigated. The question arises whether the stiffness of a polymer chain might induce differences between the longitudinal and lateral tube dimensions. An ideal candidate is syndiotactic polypropylene (s-PP), which shows a significantly larger stiffness than the other investigated polymers and a sufficiently high mobility for NSE experiments. The underlying notion is that if due to the high stiffness of s-PP, the ratio of longitudinal confinement and lateral tube diameter is significantly larger compared to the other investigated polymers, two independent length scales determine the restriction of motion in long-chain polymer melts.

The stiffness parameter C_∞ for s-PP is considerably higher than those for other polymers. Experimentally determined values from the literature cover a range of $C_\infty = 6.8$ at 448 K[9] to $C_\infty = 9.2$ at 463 K,[10] all for samples with a polydispersity of ∼2 or higher. In simulations, even higher values were found; $C_\infty = 11.7$ for MC simulations at 450 K[11] and $C_\infty \approx 11$ for MD simulations at 473 K.[12] Until recently, a narrowly distributed s-PP was not available. For the underlying work, fully protonated and deuterated s-PP with a high molecular weight has been successfully synthesized. The dynamic moduli and the dynamic structure factors have been measured. The data were analyzed in terms of standard Rouse and reptation models as well as with the recently developed method. In Section II, the models are briefly recapped, and in Section III, the experimental details are given. The data are analyzed in Section IV and discussed in Section V, with a summary in Section VI.

II. THEORY

II.I. Modeling of Dynamic Structure Factors. Neutron scattering provides access to the polymer dynamics (and structure) directly at the level of the chains. In this work, we have studied both the segment−segment pair-correlation function within a labeled chain in the melt as well as the segment self-correlation function (here, we take the monomer as the chain segment). Studying a labeled chain in the melt gives rise to coherent scattering monitoring the pair-correlation function; in terms of the Gaussian approximation for the intermediate scattering function we get

$$S_{\mathrm{coh}}(q, t) = \frac{1}{N}\sum_{m,n}^{N} \exp\left(-\frac{q^2}{6}\langle (r_m(t) - r_n(0))^2\rangle\right) \tag{1}$$

The sum runs over all segments m, n at different times $t = 0$ and t within a given chain, q is the momentum transfer, and N is the number of monomers or segments within the chain. The segmental mean-squared displacement (MSD) may then be calculated, e.g., in the framework of the Rouse dynamics,[4] which considers a chain in a heat bath or the local reptation picture, as provided by de Gennes[13] and further developed by Monkenbusch et al.[7]

By incoherent scattering, the segment self-correlation is measured. For a Gaussian chain with Rouse dynamics, the incoherent scattering function is given by

$$S_{\mathrm{inc}}(q, t) = \exp\left(-\frac{q^2\langle r^2(t)\rangle}{6}\right) \tag{2}$$

with the segmental mean-squared displacement $\langle r^2(t)\rangle = \sqrt{4\frac{Wl^4 t}{\pi}}$, where the Rouse rate $W = \frac{3kT}{\xi l^2}$ is determined by the segmental friction ξ and the temperature T; l is the segment length.

The Rouse model applies to short unentangled chains and to long entangled chains at early times below the entanglement time τ_e. The entanglement time is the Rouse time of a chain with the end-to-end distance $R_e^2 = N_e l^2$, with N_e being the number of segments between two entanglements. Around that time scale, the segments start to feel the constraints by the other chains, which are described in the reptation model by a virtual tube confining a given chain to a one-dimensional Rouse motion along the tube profile, so-called local reptation, and a slow diffusive creep motion out of the tube. In the standard reptation model by de Gennes, the dynamic structure factor is then

$$S(q, t) = [1 - F(q)]S_{\mathrm{loc}}(q, t/\tau_0) + F(q)S_{\mathrm{esc}}(q, t/\tau_d) \tag{3}$$

with $F(q) = \exp(-(qd/6)^2)$ usually taken as an approximation of a tube form factor[14] with the lateral tube diameter d identified with the distance between two entanglements and equal to the tube step length $d = \sqrt{N_e l^2}$; τ_0 and τ_d are the time scales for local reptation and the terminal time of the reptation process, respectively. Equation 3 neglects the Rouse motion lateral to the tube profile. Within the accessible NSE time window, the creep motion out of the tube is too slow to be observed, so that $S_{\mathrm{esc}} = 1$. For shorter chains, reptation limiting processes such as contour length fluctuations[3] might become visible within the NSE window.[15]

In a recent paper,[7] de Gennes' reptation model has been further developed. Besides refining the local reptation contribution, the Rouse dynamics within the tube has also been incorporated by introducing a "Rouse blob" of size $R_e = f\sqrt{N_e l^2}$, with the longest relaxation time $\tau_e = R_e^4/(\pi^2 W l^4)$, describing the lateral Rouse motion within the tube; f is a proportionality factor, which, if different from 1, allows for an assessment of a potential asymmetry of the tube. Based on previous experimental findings,[16,17] non-Gaussian effects were also included for the Rouse blob motion. In her theoretical paper, Guenza[18] came to the conclusion that the chain dynamics is non-Gaussian, which she described in terms of a non-Gaussian parameter $\alpha(t)$. The scattering function for the Rouse blob then becomes

$$S(q, t) = \frac{1}{N_{\mathrm{blob}}}\sum_{i,j}^{N_{\mathrm{blob}}} \exp\left[-\left(\frac{q^2}{6}\right)f(q^2)\langle [r_i(t) - r_j(0)]^2\rangle\right] \tag{4}$$

with

$$f(q^2) = 1 - q^2\alpha(t)\langle [r_m(t) - r_m(0)]^2\rangle/12 + O(q^4)$$
$$\cong \exp(-q^2\alpha(t)\langle [r_m(t) - r_m(0)]^2\rangle/12)$$

https://doi.org/10.1021/acs.macromol.3c02529
Macromolecules 2024, 57, 3098−3108

and

$$\langle [r_m(t) - r_m(0)]^2 \rangle = \frac{4N_{blob}l^2}{N_{blob}\pi^2} \sum_{m,p}^{N_{blob}} \frac{1}{p^2} \cos\left(\frac{p\pi m}{N_{blob}}\right)^2 \left[1 - \exp\left(-2W\left(1 - \cos\left(\frac{p\pi}{N_{blob}}\right)\right)t\right)\right]$$

Motivated by Guenza's simulation findings, a logarithmic Gaussian function for the non-Gaussian parameter $\alpha(t) = \alpha_0 \exp[-((\ln t - \ln t_{max})^2/(2\sigma^2))]$ has been introduced with $\alpha_{max} = \alpha_0$, $t_{max} = \tau_e$, and σ, the width of the distribution.

II.II. Modeling of the Static Structure Factor. In small-angle neutron scattering (SANS), the measured intensity is proportional to the macroscopic differential scattering cross section. This is connected through a contrast factor with the static structure factor $S(q, t = 0)$. As the used samples consist of a mixture of deuterated and protonated chains, both with a nearly bimodal molecular weight distribution (see Section III.I), the random phase approximation (RPA) for a 4-component system was considered.[19,20] As will be shown later, the specific interactions between deuterated and protonated segments are unmeasurably small; therefore, the Flory–Huggins interaction parameter is fixed to zero. The macroscopic differential scattering cross section for a 4-component system of shorter and longer protonated and deuterated chains (labeled h/H and d/D) is then

$$\frac{d\Sigma(q)}{d\Omega} = \Delta\rho^2 \frac{[S^0_{hh} + S^0_{HH}]\cdot[S^0_{dd} + S^0_{DD}]}{S^0_{hh} + S^0_{HH} + S^0_{dd} + S^0_{DD}} = I_{RPA} \quad (5)$$

with $\Delta\rho^2$ the scattering contrast between deuterated and protonated s-PP, and the single static structure factors $S^0_{ii}(q, l) = N_i\varphi_i v_i P_i(q, l)$ with the number of monomer (= segments) N_i, volume fractions φ_i, and monomer volumes v_i of the different components in the mixture. $P_i(x)$ are the Debye functions for Gaussian chains, $P_i(x) = \frac{1}{x^2}(e^{-x} - 1 + x)$ with $x = q^2R^2_{g,i}$, with the radii of gyration $R^2_{g,i} = \frac{1}{6}N_i l^2$ allowing to determine the monomeric statistical segment length l.

II.III. Modeling of Dynamic Moduli. The standard model to describe the dynamic moduli of linear polymers is the Likhtman–McLeish model.[21] It provides basic parameters such as plateau modulus and entanglement time. Due to the onset of crystallization of s-PP in the interesting and required temperature range, however, the accessible frequency window is quite limited and does not allow a reliable determination of the different unknown parameters. Therefore, the dynamic modulus has been described by the empirical BSW model,[22] which assumes a continuous relaxation spectrum $H(\tau)$ to describe the storage and loss modulus

$$G'(\omega) = \int_{-\infty}^{+\infty} H(\tau)\omega^2\tau^2/(1 + \omega^2\tau^2)d(\ln \tau)$$

$$G''(\omega) = \int_{-\infty}^{+\infty} H(\tau)\omega\tau/(1 + \omega^2\tau^2)d(\ln \tau)$$

The spectrum combines entangled and glassy regime in the form of $H(\tau) = H_e\tau^{n_e} + H_g\tau^{-n_g}$ for $\tau_0 < \tau < \tau_{max}$ and $H(\tau) = 0$ outside this range, with $H_e = n_e G^0_N \tau^{-n_e}_{max}$ and $H_g = n_g G^0_N \tau^{n_g}_0$. The spectrum is thus limited to the range between a minimum time τ_0 and maximum time τ_{max}, the latter related to thedisentanglement time τ_d. n_e and n_g are the slopes in the respective regimes. The Rouse/glassy regime at high frequencies was not accessible in our experiment, but nevertheless, from the low-frequency entangled regime, the plateau modulus G^0_N can be obtained. From the pure reptation model, $n_e = 1/2$ is expected but crosses over to $n_e = 1/4$ if contour length fluctuations relax the chains faster than reptation out of the tube does. It changes the effective slope of the high-frequency wing of the terminal loss peak for not too long polymers. The Likhtman–McLeish model provided the physical background for the alleged universal value for $n_e = 1/4$. The plateau modulus contains the length scale of tube confinement $G^0_N = \frac{\rho RT}{M_e}$ with M_e the entanglement molecular weight and ρ the density.

III. EXPERIMENTAL METHODS

III.I. Sample Preparation. Syndiotactic polypropylene has been synthesized by highly syndiospecific living olefin polymerization.[23] Three different samples were prepared: For the SANS and coherent NSE experiments, a set of protonated and deuterated s-PP was synthesized, with the protonated sample also being used for the backscattering spectroscopy. For the incoherent NSE measurement, a second fully protonated sample has been synthesized. The procedure for the first set of samples (protonated resp. deuterated) is as follows: In a glovebox, a 6 oz Lab-Crest pressure reaction vessel (Andrews Glass) equipped with a magnetic stir bar was charged with dried PMAO (Albemarle; 435 mg, 7.5 mmol Al) and toluene (150 mL). The reaction vessel was brought out of the glovebox and cooled to −78 °C in a dry ice/acetone bath. The reactor atmosphere was exchanged with propylene resp. propylene-d_6 three times, and then the solution was saturated under pressure (40 psi). The reactor was then closed to propylene and warmed to 0 °C. The titanium catalyst (bis[2,4-bis(1,1-dimethylethyl)-6-[[(2,3,4,5,6-pentafluorophenyl)-imino-κN]methyl]phenolato-κO]dichlorotitanium;[23] 46 mg, 0.050 mmol) was dissolved in toluene (4 mL) at room temperature under nitrogen, and the solution was added to the reactor via a gastight syringe to initiate the polymerization. The polymerization was allowed to proceed for 20 h or 16.5 h at 0 °C. The reactor was vented, and the polymerization was quenched by addition of methanol (MeOH). The polymer was precipitated in 5% HCl/MeOH, filtered, washed with MeOH, and then dried in vacuo to a constant weight. The procedure for the second protonated s-PP was the same except for the amount of dried PMAO (870 mg, 15.0 mmol Al) and titanium catalyst (91.5 mg, 0.100 mmol, dissolved in 8 mL of toluene), and the reaction vessel was cooled down to only 0 °C in an ice bath, and the polymerization proceeded for 24 h.

All samples have been characterized by absolute gel permeation chromatography (GPC) measurements with both light-scattering detection and refractometer (filtered with 0.45 μm filter in trichlorobenzene, 135 °C, Dow, Benelux) (see the Supporting Information (SI)). This revealed a skewed or bimodal distribution for the first protonated and deuterated samples. The molecular weight was estimated to be about 45% 105 kg/mol and 55% 200 kg/mol for the deuterated s-PP and about 40% 105 kg/mol and 60% 174 kg/mol for the protonated component. The overall polydispersity index was $M_w/M_n \sim 1.37–1.39$. For the second protonated s-PP sample (for the incoherent NSE measurements), the absolute GPC measurement gave a molecular weight of 109 kg/mol with comparable polydispersity of 1.4.

For the different measurements, the samples have been stabilized with dibutylhydroxytoluene (BHT) as the antioxidant. For the SANS measurements, a mixture of 1, 2, and 3 mass% deuterated s-PP in protonated s-PP was compression-molded under vacuum and filled into quartz sandwich cells with a copper frame, where the 2% mixture has also been used for the rheological measurements. For the coherent NSE measurement, a mixture of 10% protonated chains in a

https://doi.org/10.1021/acs.macromol.3c02529
Macromolecules 2024, 57, 3098−3108

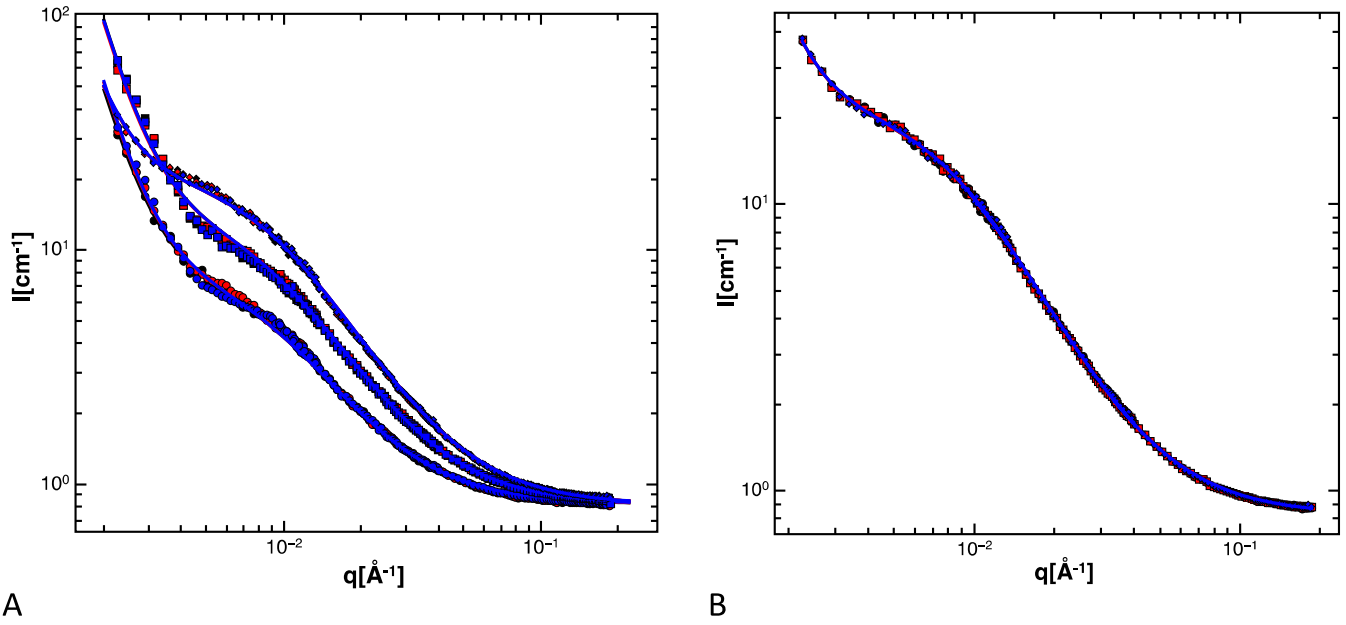

Figure 1. Measured SANS intensity in dependence of q. (A) Simultaneous fit (lines) to all temperatures (black 453 K, red 463 K, blue 473 K) and concentrations (circles 1%, squares 2%, diamonds 3%). (B) Simultaneous fit (line) to all temperatures (black circles, 453, red squares, 463, blue diamonds, 473 K) for the 3% sample only.

deuterated matrix has been used, sealed under an inert atmosphere in a standard niobium container. For the backscattering and incoherent NSE measurements, pure protonated samples have been used in sealed aluminum containers.

III.II. Rheological Measurements. The linear viscoelastic properties of the syndiotactic polypropylene were measured on an ARES rheometer (Rheometric Sci) using a 2K FRNT transducer in oscillatory shear in parallel plate geometry with a diameter of 8 mm. Isothermal frequency sweeps between 0.01 and 100 rad/s and temperatures varying from 160 to 120 °C in steps of 10 °C were performed on a sample of about 1 mm thickness. A liquid nitrogen blanket prevented accidental oxidation during the measurements. Master curves at the reference temperature T_0 = 160 °C were generated by a two-dimensional shifting algorithm using the instrument software. Average C_1 and C_2 factors from the limited number of temperatures were determined from fitting the WLF equation $\log a_T = -C_1(T - T_0)/(C_2 + (T - T_0))$ to the temperature-dependent shift factor a_T.

III.III. Neutron Scattering. The use of neutron scattering allows access to the structure and dynamics of the polymer chains directly on a molecular level. Protons and deuterons have different neutron scattering lengths, providing contrast to measure the coherent (dynamic) structure factor. For fully protonated samples, one measures the incoherent dynamic structure factor, i.e., the self-correlation function of the segments. The momentum transfer q in the (quasi-) elastic case relates to the neutron wavelength λ as $q = (4\pi/\lambda)\sin(\Theta/2)$, with Θ being the scattering angle.

(i) Small-angle neutron scattering (SANS): For the determination of the statistical segment length and stiffness parameter, the static structure factors for three different concentrations (1, 2, 3%) of deuterated chains in a protonated matrix and three temperatures (463, 473, 483 K) have been measured. Samples were contained in copper−quartz cells and placed in an electrical furnace under vacuum. The experiments have been performed at the KWS-1 instrument at the Jülich research reactor FRJ-2. The measurements have been done at 3 detector distances (2, 8, 20 m) at a neutron wavelength of 7 Å with 20% dispersion covering a q-range of about 0.002−0.2 Å^{-1}.

(ii) Neutron backscattering spectroscopy (BSS): For the independent determination of the Rouse rate, a fully protonated s-PP melt was studied by neutron backscattering using the neutron backscattering spectrometer BSS at the Jülich research reactor FRJ-2. The quasi-elastic spectra were measured for three different temperatures (463, 473, and 483 K) at a neutron wavelength of 6.2 Å covering a q-range of 0.2−1.9 Å^{-1}. The instrumental resolution is mainly determined by the monochromator/analyzer crystals (Si111) and is about 1 μeV (fwhm), as measured with a standard vanadium sample. By motion of the monochromator, a Doppler shift of the incoming neutron wavelength is achieved, providing a dynamic range of ±17 μeV. The data were normalized and corrected for background from an empty sample holder.

(iii) Neutron spin echo spectroscopy (NSE): NSE spectroscopy yields the intermediate scattering function $S(q,t)/S(q)$. To measure the segmental and chain dynamics, two different NSE experiments have been performed. For 10% protonated chains in a deuterated matrix, the single-chain dynamic structure factor is measured, revealing the segment−segment pair correlations within the labeled polymer. This was measured with the IN15 NSE spectrometer at the Institut Laue-Langevin at a temperature of 473 K and a wavelength of 15 Å, covering a q-range of 0.03 to 0.115 Å^{-1} and a time range up to 170 ns. The data were corrected for resolution and background; the latter was obtained from a fully deuterated sample.

For a fully protonated sample, the incoherent dynamic structure factor is observed, which yields the segment self-correlation. The incoherent NSE measurements were performed at the J-NSE operated by JCNS at the Heinz Maier-Leibnitz Zentrum (MLZ) in Garching,[24] at a temperature of 473 K. A set of 3 q-values (0.1−0.15 Å^{-1}) at a wavelength of 8 Å was measured up to ∼40 ns. To further extend the accessible time range up to about 120 ns, an experiment at 12.8 Å for a q-value of 0.07 Å^{-1} has been done. The data were corrected for resolution and background; the latter was obtained from an empty sample holder.

IV. RESULTS

IV.I. SANS. For all of the samples in the temperature range of 453−473 K, the SANS pattern did not depend on temperature. At low q-values, all samples displayed a strong

https://doi.org/10.1021/acs.macromol.3c02529
Macromolecules 2024, 57, 3098−3108

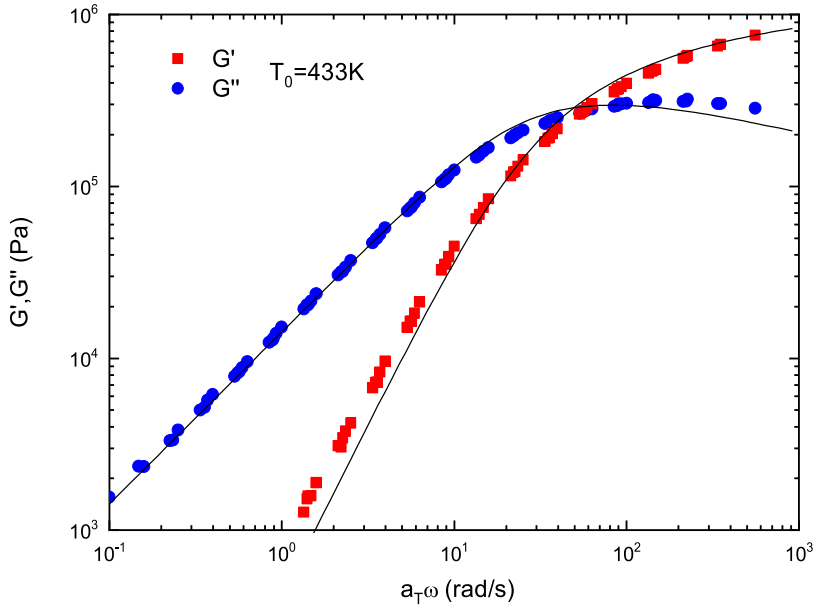

Figure 2. Measured storage (red squares) and loss (blue circles) modulus for the 2% mixture for a reference temperature of 433 K. Lines are a fit with the BSW model.

forward scattering. There, the scattered intensity follows approximately a $\sim q^{-4}$ dependence, indicating that it might stem from surface or Porod scattering from microscopic voids within the sample, overlaid by the polymer form factor. After subtracting the different incoherent background levels, the concentration-dependent scattering intensity can be accounted for by normalizing the resulting data with the corresponding volume fraction $\phi(1-\phi)$ for each sample. Then, all data overlap, except for the excess forward scattering at low q due to the randomness in the origin of parasitic scattering. We do not observe any influence from a Flory–Huggins parameter between hydrogenated and deuterated species, and a common RPA-function can be fitted for all three samples simultaneously.

Considering the bimodal molecular weight distribution of both deuterated and protonated chains, a 4-component RPA model is used (eq 5) to fit the data. Including the incoherent background and the forward scattering, the full fit function is then $I(q) = I_0 I_{RPA}(q, l) + I_1 q^{-4} + I_2$ with I_i intensity factors.

The resulting simultaneous fits are very good and result in a monomer length of l = 7 Å (Figure 1A). Fitting additionally the exponent of the forward scattering improves the fits only marginally but then yields l = 7.2 Å. Since for the two lower concentrations the fits are slightly but visibly worse than for the 3% sample, where the least parasitic scattering is observed and the polymer contribution at low q is the highest, we limited the fit to the highest concentration (Figure 1B). This yields a segment length of l = 7.43 Å, which also does not vary so strongly anymore with the exponent of the forward scattering: if the exponent of the power law is fitted (yielding −4.3), the variation of l to 7.48 Å is within the accuracy of determination. The fitting error is smaller than 0.5%, but the systematic error, e.g., due to uncertainties in molecular weight distribution, is larger (on the order of few %). This value is also close to the literature value of 7.6 ± 0.3 Å.[25]

The stiffness parameter C_∞ can be determined from the relation $l^2 = C_\infty n l_0^2$ with n the average number of main-chain bonds per monomer (2) and l_0 the average bond length (1.54 Å). With l = 7.4 Å, the stiffness parameter C_∞ becomes 11.5, somewhat larger than the literature value of 9.2[10] and in line with findings from simulation, where, dependent on the method, C_∞ is in the range of ∼11 (MD)−11.7 (MC).[11,12] Knowing the length l, the ratio of the end-to-end distance to molecular weight can also be calculated: $\frac{\langle R_e^2\rangle}{M} = \frac{Nl^2}{M} = 1.3\ \text{Å}^2\text{mol}/g$. With that, the packing length[26,27] can be obtained: $p = \frac{M}{\langle R_e^2\rangle \rho N_A}$, with ρ the density and N_A the Avogadro constant, resulting in p = 1.68 Å. Compared to other polymers, s-PP is quite stiff (large C_∞), but the packing length, which is the ratio of the occupied chain volume to chain dimension, is small.

IV.II. Rheology. As syndiotactic polypropylene crystallizes, it was not possible to measure the full modulus, only the terminal flow regime was covered, showing the characteristic loss peak of $G''(\omega)$. Although the sample has a close to bimodal molecular weight distribution, the distribution for each component is quite narrow. The peak molecular weights differ roughly by a factor of 2, so that the terminal times should be well separated by at least a factor of $\sim 2^3 = 8$ on the frequency axis. Therefore, a fit of the data with the BSW ansatz was possible; fixing the slope n_e to 1/4 results in a modulus of 1.15 MPa at 433 K (see Figure 2). With $G_N^0 = \frac{\rho RT}{M_e}$ and a density of 0.76 g/cm^3, the entanglement molecular weight is then ∼2.4 kg/mol. In the literature, a value of G_N^0 = 1.35 MPa at 463 K with then M_e = 2.2 kg/mol is reported.[28] Liu et al.[29] argued that the value of the plateau modulus is overestimated due to the used extrapolation. They determined the plateau modulus with different methods, obtaining an average value of G_N^0 = 0.87 MPa at 463 K with then M_e = 3.37 kg/mol. Combining our result with the result from SANS for $\frac{\langle R_e^2\rangle}{M} = 1.3\ \text{Å}^2\text{mol}/g$, the rheological tube diameter can be determined from $\frac{d^2}{M_e} = \frac{\langle R_e^2\rangle}{M}$ as d = 56 Å.

IV.III. BSS. Neutron backscattering spectroscopy was used to observe the local segmental motion. In principle, the methyl groups of the polymer also contribute to the dynamics, but at

https://doi.org/10.1021/acs.macromol.3c02529
Macromolecules 2024, 57, 3098−3108

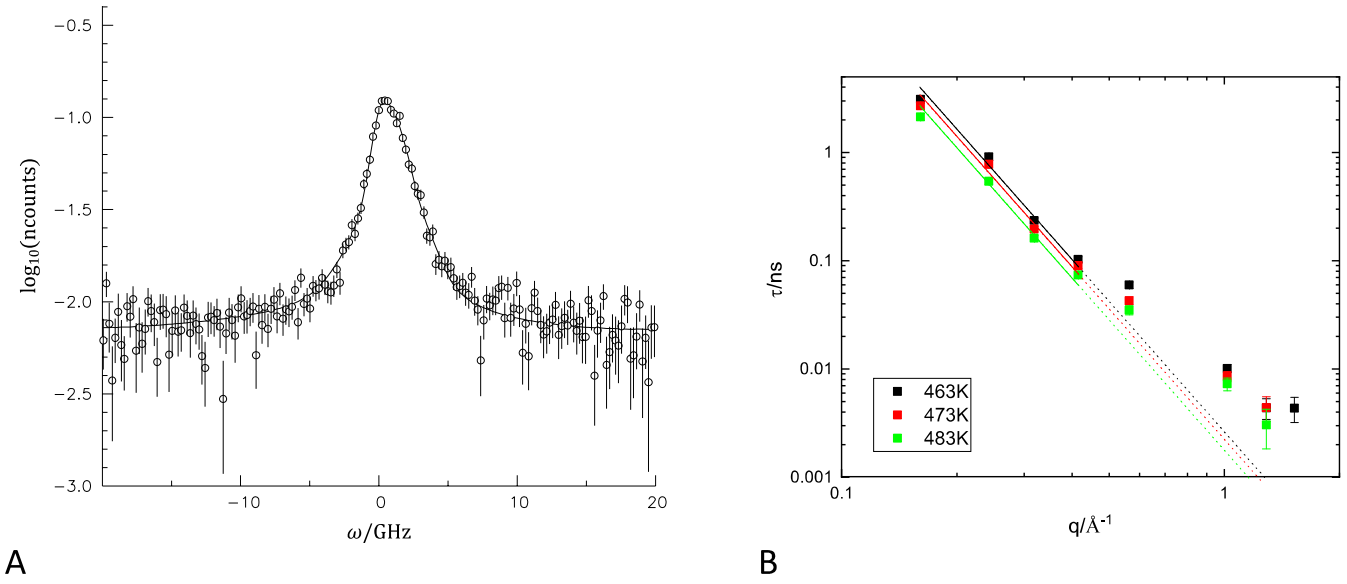

Figure 3. (A) Example of backscattering data for T = 473 K and q = 0.16 Å^{-1} (symbols) with the KWW fit (line). (B) log−log plot of fitted time scale vs q (symbols) for the 3 different temperatures with linear fits (solid lines) for the first 4 q-values.

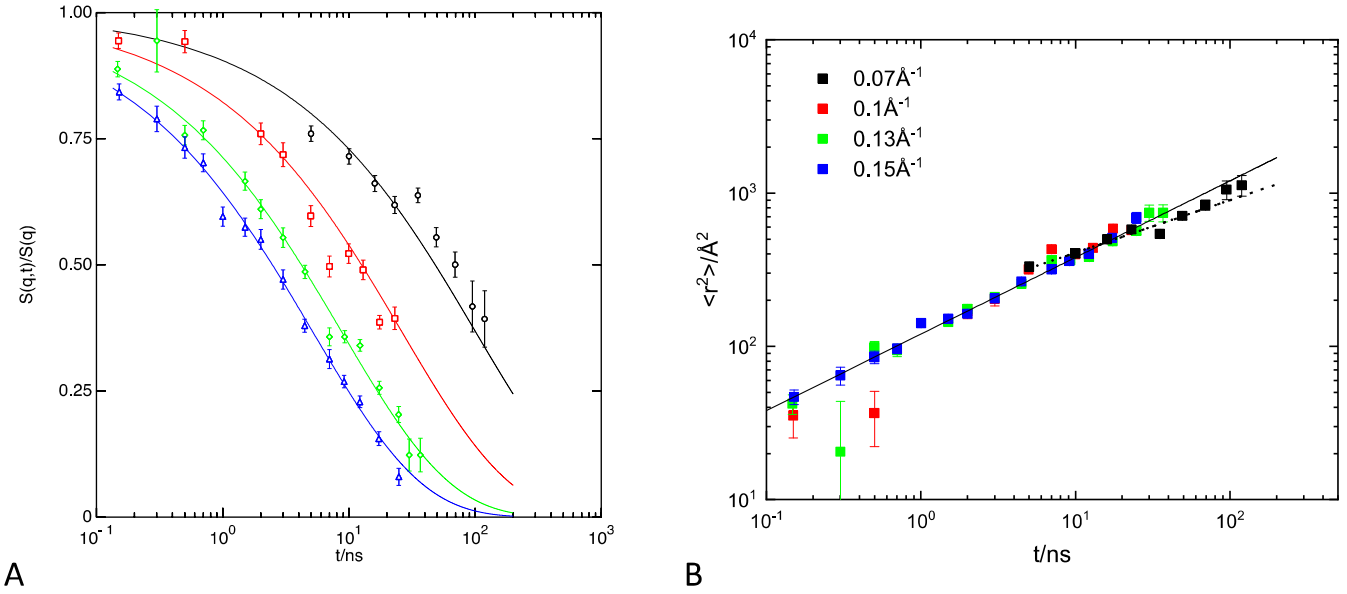

Figure 4. (A) Incoherent NSE data for T = 473 K and q = 0.07, 0.1, 0.13, and 0.15 Å^{-1} (symbols top to bottom) with a fit of the incoherent Rouse function (lines). (B) Extracted mean-squared displacement for the same data with the Rouse expectation (solid line $\sim t^{1/2}$) and fitted power law for the smallest q-value (dotted line $\sim t^{0.34}$).

elevated temperatures, where the measurements were performed, the methyl group rotation is too fast for the accessible dynamic window. After the subtraction of the empty cell, no elastic contribution remains. Hence, the observed quasi-elastic broadening can be described by one stretched exponential function (KWW) $S(q, t) = \exp\left[-\left(\frac{t}{\tau}\right)^{\beta}\right]$ with the stretching exponent β = 0.5 (Rouse expectation). The measured scattering intensity is a convolution of the polymer scattering function with instrumental resolution. The measured instrumental resolution is fitted with a sum of Gaussian functions, which then gives easy analytic access to the Fourier transform time domain resolution. The convolution with the resolution is then performed by multiplying the time-dependent model function with the Fourier transform of the fitted resolution function and then back-transformed to the frequency domain by numerical Fourier transformation.[30] The relaxation time has been fitted for each q-value independently (see Figure 3A). At higher q-values, the quasi-elastic signal is too broad for the limited dynamic range to be fitted. At low q, the relaxation times follow a q^{-4} dependence, as expected for Rouse dynamics: $\tau = 9\pi/(Wl^4)\cdot q^{-4}$ (see Figure 3B). Limiting the fit to q < 0.5 Å^{-1} where this relation is fulfilled, the Rouse parameter Wl^4 can be extracted. Only a weak temperature dependence was observed; for the explored temperature range, Wl^4 varies from about 10700 to 15900 Å^4/ns. At 473 K where the NSE measurements have been performed, the Rouse parameter is Wl^4 = 12620 ± 1160 Å^4/ns.

IV.IV. Incoherent NSE: Dynamic Self-Correlation. On a hydrogenated sample, the NSE experiment measures the

https://doi.org/10.1021/acs.macromol.3c02529
Macromolecules 2024, 57, 3098−3108

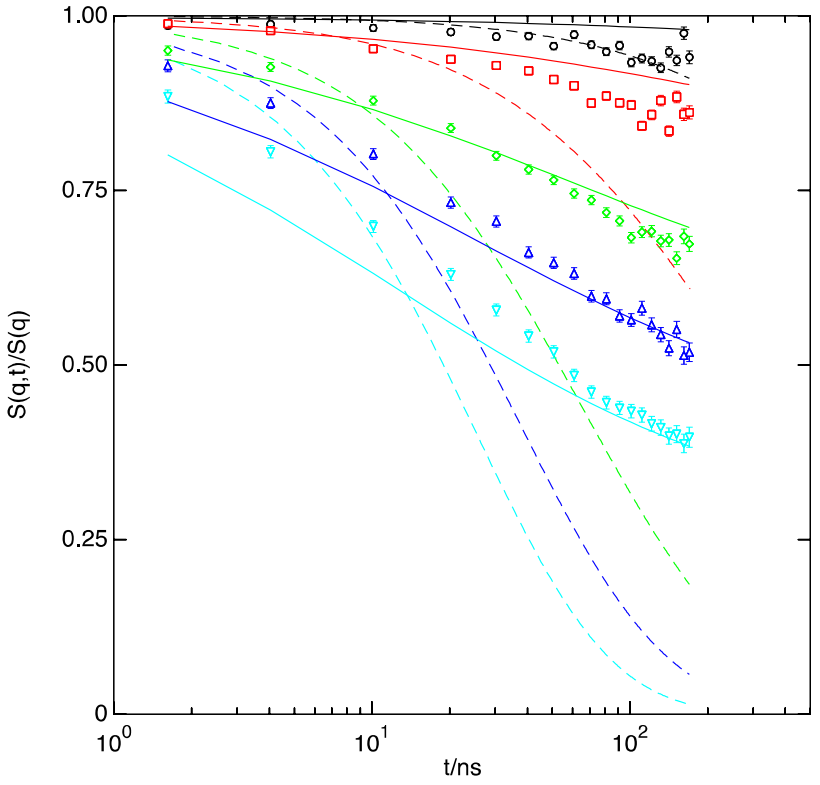

Figure 5. Measured single-chain dynamic structure factor for T = 473 K and q = 0.03, 0.05, 0.077, 0.096, 0.115 Å^{-1} (symbols top to bottom), including a fit of the Rouse model (dashed lines) and standard de Gennes model (local reptation) (solid lines).

incoherent dynamic structure factor in the time regime. As for the case of the backscattering measurements at lower q, the data is well described by the Rouse function for self-correlation in the explored q and t range (Figure 4A). Only at longer times (only measured for the smallest q) does there seem to be some deviation. Taking the segment length from SANS (l = 7.4 Å) and fitting the Rouse parameter for times t < 40 ns result in a value of Wl^4 = 11525 ± 195 Å^4/ns, close to the result from backscattering spectroscopy, demonstrating the consistency of measurements in energy and time space. The mean-squared displacement $\langle r^2\rangle = \frac{-6}{q^2}\ln(S(q,t)/S(q,0))$ extracted from the measured dynamic structure factor displays a time dependence $\sim t^{1/2}$ over most of the accessible time range, as expected for Rouse dynamics (Figure 4B). Only the last few points seem to deviate from this power law. When the segments reach the tube confinement at the entanglement time τ_e, a change in slope to a power law $\sim t^{1/4}$ is expected. As was already seen for other polymers, this crossover in the MSD signifying τ_e from incoherent NSE data appears at much lower time values than determined from coherent NSE data.[5] But a good fit with a slope of 1/4 for the last points could not be achieved. In order to find a trend, we fitted only the lowest q data covering the time range ∼5−120 ns. There, a power law $\sim t^{0.34\pm0.04}$ is found, which crosses the Rouse line at about 20 ns (dotted line Figure 4B). Although no clear $\sim t^{1/4}$ range was found, taking the observed deviation as a crossover from Rouse dynamics to local reptation seems to be in agreement with the findings from the coherent NSE measurements with τ_e on the order of 100 ns (see Section IV.V).

IV.V. Coherent NSE: Dynamic Pair Correlation. The coherent NSE experiment measures the single-chain dynamic structure factor. Neither the Rouse model at early times (with the Rouse rate from incoherent NSE) nor the commonly used de Gennes reptation model (with tube diameter fitted) at longer times describes the data at all (Figure 5). Also, limiting the reptation fit to times >80 ns does not yield a satisfactory description of the "plateau" levels; the fitted tube diameter changes from 61 to 63 Å. Fitting the plain Rouse model for times <15 ns gives a too large Rouse parameter of about 31000 Å^4/ns without describing the data beyond the fit range (except for the smallest q-value). Fitting both tube diameter (141 Å) and Rouse rate (1710 Å^4/ns, way too small) in the reptation model gives the best fit results but still no satisfactory description of the data. Also, considering contour length fluctuations (CLF)[15] does not improve the fits.

In a next step, the data has been fitted with the extended de Gennes model:[7] In order to reduce the number of parameters, as many parameters as possible were fixed: the segment length to 7.4 Å from SANS, the Rouse parameter to 11525 Å^4/ns from the incoherent NSE measurement, and the number of segments = monomers ∼2500. The bimodal molecular weight distribution does not play an important role here: using the number of segments of the longer chain does not markedly change the fit results. The model considers a generalized local reptation with a Rouse blob and CLF contribution. The effect of CLF here is marginal, as the chains are long and only contribute at large times. Additional non-Gaussianity contributions are included, with $\tau_{max} = \tau_e$ and σ = 1 if not noted otherwise. In order to obtain a good description of the data an asymmetry factor f between the tube step length $d = l\sqrt{N_e}$ and the lateral tube dimension characterized by the end-to-end distance of the Rouse blob $R_e = fl\sqrt{N_e}$ was also considered. In the standard tube model, f = 1, with the tube diameter corresponding to the tube step length. With an asymmetry

https://doi.org/10.1021/acs.macromol.3c02529
Macromolecules 2024, 57, 3098−3108

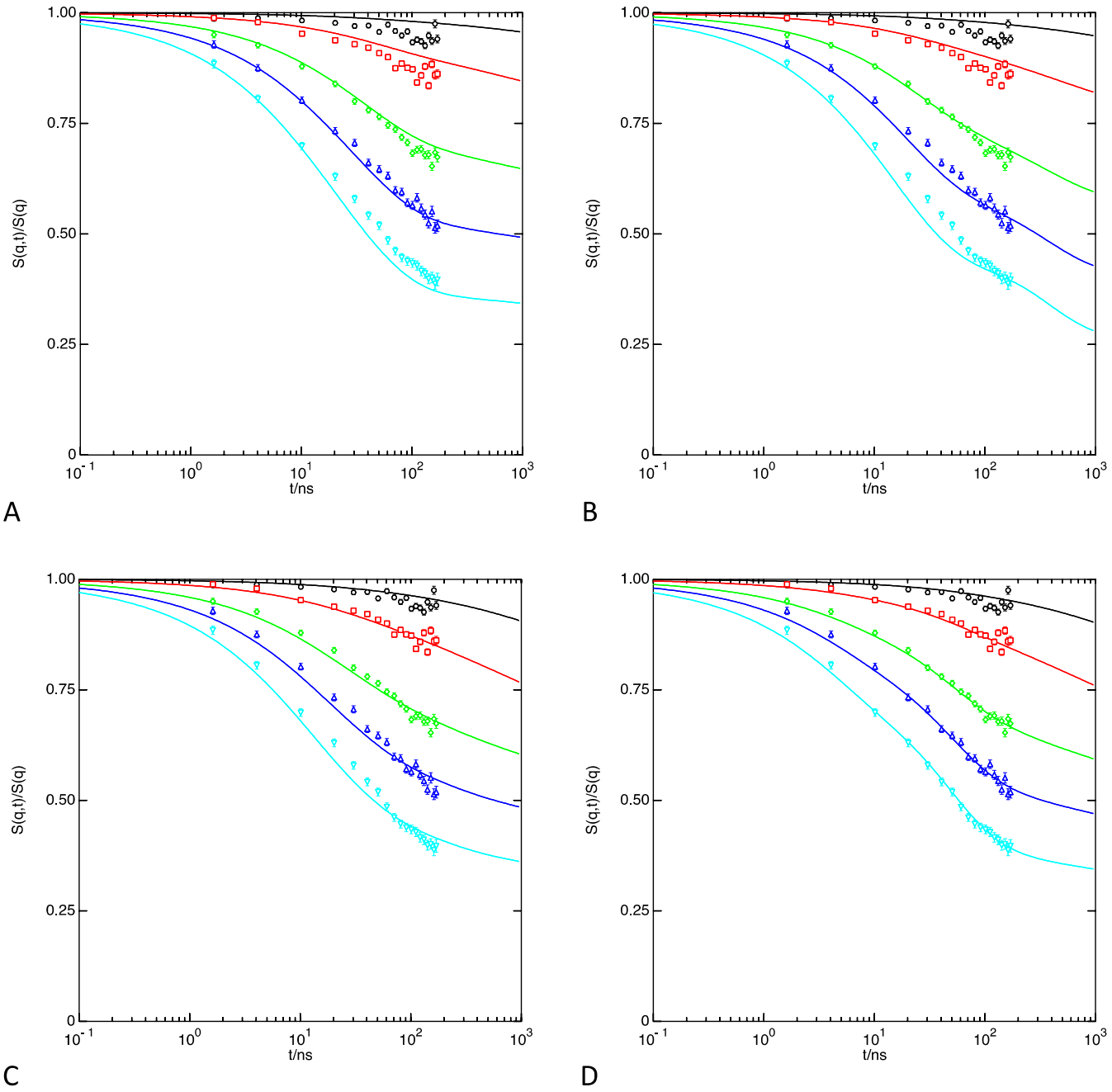

Figure 6. Coherent NSE data for T = 473 K and q = 0.03, 0.05, 0.077, 0.096, 0.115 Å^{-1} (symbols top to bottom) with a fit of the Monkenbusch model (s. text). (A) Plain fit, (B) NG α_0 fitted, (C) additional asymmetry factor f fitted, and (D) same as part (C) but with τ_{max} set to 0.3τ_e.

factor different from 1, an effective tube diameter may be calculated: $d_{eff} = \sqrt{\frac{1}{3}(d^2 + 2R_e^2)} = l\sqrt{\frac{1}{3}N_e(1 + 2f^2)}$. For $f = R_e/d < 1$, the tube is narrower in the lateral direction.

Already with the plain extended de Gennes model, an improved fit is obtained but still deviations, in particular, of the q-dependence are visible (Figure 6A). The only fitting parameter is d, yielding a value of d = 58 Å; all other parameters are fixed. In line with previous findings,[7] the influence of non-Gaussian (NG) effects was tested: allowing additionally for a finite amplitude α_0 in the fitting, only a marginal improvement is obtained (Figure 6B). The NG correction is small but leads to an unphysical "bump" at large q and long times around τ_{max} due to the neglect of unknown $O(q^4)$ terms in eq 4. Fitting additionally the width of the NG contribution and/or lowering τ_{max} does not improve the consistency of the fit (see the SI). A good description of the data with reasonable parameters is only obtained when the asymmetry factor f between lateral and longitudinal tube dimensions is also allowed. The fitted tube step length is then d = 106 Å, and the asymmetry factor f = 0.51, with only a very small contribution of NG (Figure 6C). Nevertheless, some deviations at intermediate times are still visible. Setting τ_{max} = 0.3τ_e and fitting d, α_0, and f, a very good description of the data is obtained (Figure 6D). The NG contribution is increased, but the other parameters are hardly changed. The asymmetry factor is quite high, and the effective tube diameter is then 78 Å. Fitting also τ_{max} results in a value of 0.25τ_e without

https://doi.org/10.1021/acs.macromol.3c02529
Macromolecules 2024, 57, 3098−3108

Table 1. Fit Results and Resulting Parameters[a]

fit	N_e	α_0	f	d [Å]	R_e [Å]	d_{eff} [Å]	τ_e [ns]	ssq
A: plain	62	0	1	58	58	58	100	13.4
B: +NG α_0	75	0.11	1	64	64	64	147	10.9
C: +NG + asym f	204	0.04	0.51	106	54	75	76	4.7
D: C with $\tau_{max} = 0.3\tau_e$	217	0.13	0.51	109	56	78	82	2.5

[a]N_e: number of monomers in an entanglement strand, α_0: strength of non-Gaussian correction, f: asymmetry factor, d: tube diameter, R_e: Rouse blob size, d_{eff}: effective tube diameter, τ_e: entanglement time, and ssq: χ^2 of the fit.

significantly changing the fit quality or parameters (see the SI). The fit results are summarized in Table 1.

V. DISCUSSION

Syndiotactic polypropylene is one of the cases where the dynamic structure factor for long entangled chains cannot be well described with the standard de Gennes model for local reptation. In particular, the q-dependence in the "plateau regime" is off; therefore, a direct comparison of the extracted tube diameter from the standard reptation model to the rheological value is moot. Applying the Monkenbusch model for the dynamic structure factor achieves a good description of the data, when also an asymmetry between longitudinal step length and lateral tube dimension is considered. The Monkenbusch model applied to a number of different polymers gave comparable results for the tube diameter as obtained from the standard reptation model, with the notable exception of polyisoprene (PI).[7] For all of the investigated polymers, there was an indication of an asymmetric tube, but only for PI, the asymmetry factor was considerably smaller than 1. The notion that s-PP features a more asymmetric tube as a result of its stiffness does not concur with the observation that the asymmetry for both s-PP and PI is about the same. Both polymers show a remarkably similar behavior in terms of the parameters obtained in the refined reptation model—the best fits are obtained when $f \sim 0.5$ resp. 0.4 and $\tau_{max} \sim 0.3\tau_e$. The characteristic ratio for s-PP is more than a factor of 2 larger than that for PI (see Table 2). In consequence, the

Table 2. Comparison of Characteristics and Tube Ratios for Different Polymers

polymer	C_∞	p [Å]	f	d_{rheo}/d	d_{rheo}/R_e	d_{rheo}/d_{eff}
[a]PEO	4.8	1.94	0.81	0.58	0.72	0.66
[a]PI	5	3.2	0.41	0.40	0.98	0.60
[a]PB	5.3	2.29	0.9	0.72	0.81	0.78
[a]PEP	6.4	2.52	0.88	0.67	0.75	0.72
[a]PE	7.3	1.75	1	0.63	0.62	0.63
s-PP	11.5	1.68	0.51	0.51	1.0	0.72

[a]Values from ref 7.

stiffness seems not to be the decisive factor for an asymmetric tube confinement. Also, the packing lengths p for the two polymers are nearly a factor 2 apart.

The calculated effective tube diameter accounts for the observed asymmetry (Table 1). Comparing the thus microscopically obtained effective confinement length with the rheological value for all investigated polymers, the latter value is always smaller than the NSE result (see Table 2). This is in line with the earlier similar observation with microscopic tube diameters obtained from the standard de Gennes reptation model.[7] The ratio of the rheological tube diameter to the effective tube diameter for all of the different polymers varies between ~0.6 and 0.8. The effective microscopic confinement length seems to be systematically larger than the tube diameter determined from the rheology. Looking at the ratio for longitudinal and lateral tube confinement, it is noticeable that only for s-PP and PI (where the asymmetry is largest) the rheological value is close to the Rouse blob dimension, whereas for the other polymers, this ratio also varies between 0.6 and 0.8.

In order to directly compare the different polymers, Monkenbusch et al. scaled the different spectra onto each other by using the previously determined plain model parameters of one polymer and rescaling its length and time scales to match the second polymer. They found that the q-scaling factor pertains to the ratio of the corresponding tube diameters and the time scaling to the ratio of the entanglement times. This scaling approach leaves aside any subtle NG-effects, which seem to be rather more polymer-specific.

To compare now the s-PP spectra with PE as reference data, the q-scaling factor is fitted and the time scaling factor is calculated from that $t_{scale} = \tau_e/\tau_{e,ref} = (Wl^4_{ref}/Wl^4)\cdot q^4_{scale}$. The comparison is shown in Figure 7A, and the fitted q-scaling factor is 1.21. With the scaling factors, the obtained tube diameter for s-PP from the PE reference values is 59 Å and τ_e = 106 ns, very close to the values obtained with the plain model fit. Thus, s-PP also follows the same scaling relation, but deviations are also visible, in particular, in the q-dependence. This is probably due to the highly asymmetric tube for s-PP, whereas the asymmetry factor for PE is close to 1. The deviations are similar in the case of PI compared to PE.

Thus, a comparison to PI might be useful. For PI, Monkenbusch et al. also found a similar asymmetric tube with an asymmetry parameter $f = 0.41$ compared to $f = 0.51$ for s-PP under the same fitting conditions (D). Scaling s-PP to PI, we kept the non-Gaussianity in the spectra rescaled from PI; Figure 7B presents the result. Considering both asymmetry and non-Gaussianity in the calculation of the rescaled PI-spectra leads to a nearly perfect agreement between both data. With this approach for s-PP from the fitted q-scaling factor, we obtain a tube step length of $d = d_{PI}\cdot 0.86 = 129$ Å and a lateral dimension of R_e = 53 Å, the corresponding time scaling yielding τ_e = 69 ns. We note that allowing for a slight deviation of the t-scaling from the τ_e ratio would further improve the perfection of the match. This may reflect the uncertainty in the determination of Wl^4 in the case of PI. Both values for the tube dimensions deviate somewhat from the results from the direct fits of s-PP (see Table 1), which might also be due to the slightly different asymmetry factors. Nevertheless, despite the quite different characteristic ratios, the two polymers can be well scaled to each other, again indicating that the polymer stiffness seems not to determine the observed asymmetry and that the suggested scaling properties[7] are fulfilled.

https://doi.org/10.1021/acs.macromol.3c02529
Macromolecules 2024, 57, 3098−3108

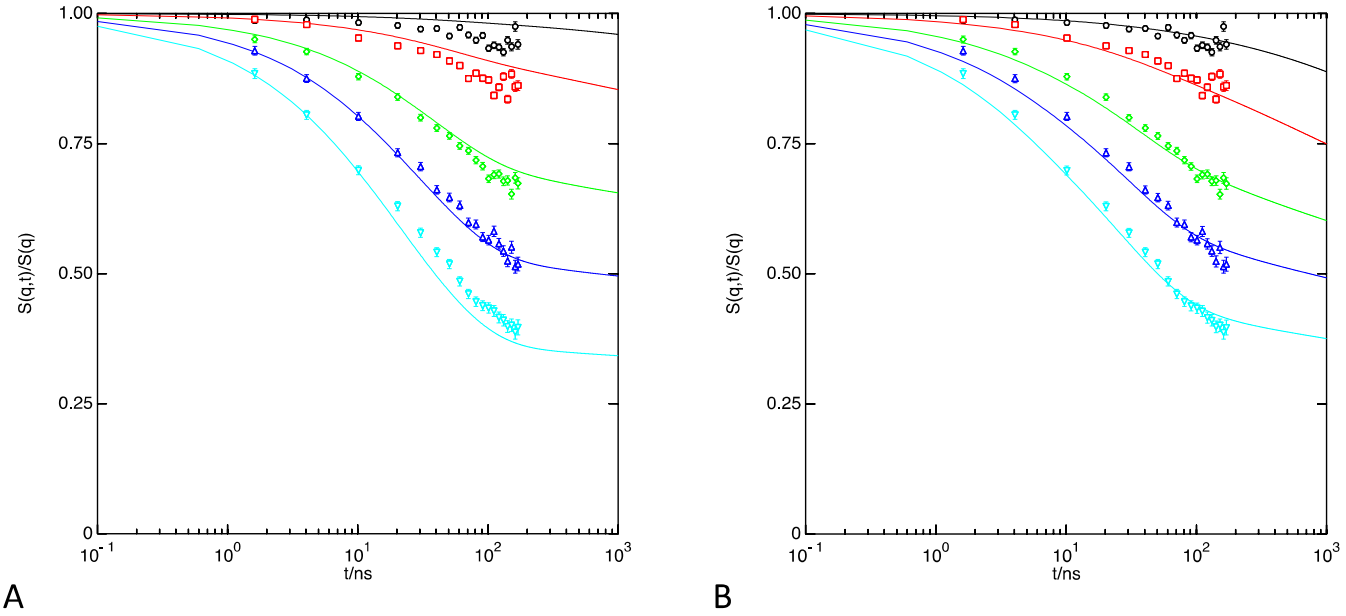

Figure 7. (A) Comparison of the scaled computed PE spectra (lines) with the s-PP data (symbols). (B) Comparison of the scaled computed PI spectra (lines) to the s-PP data (symbols).

VI. CONCLUSIONS

We have studied the structure and dynamics of long-chain syndiotactic polypropylene melts by SANS, rheology, neutron backscattering, and NSE. The investigations were performed in order to establish (i) the existence of asymmetric reptation tubes, where the step length differs from the lateral dimension and (ii) to scrutinize the hypothesis that chain stiffness generates asymmetric tubes. The following results were obtained.

- From SANS, we obtained the monomer length of s-PP l = 7.4 Å leading to characteristic ratio of C_∞ = 11.5, which is larger than that obtained from previous experiment but in good agreement with simulation.
- In the Rouse regime, neutron backscattering spectroscopy revealed that the obtained Rouse rate Wl^4 = 12620 ± 1160 Å^4/ns is in very good agreement with the corresponding result from incoherent NSE Wl^4 = 11525 ± 195 Å^4/ns.
- Incoherent NSE directly reveals the segmental MSD: for times up to about 40 ns, the MSD(t) follows the Rouse type $t^{1/2}$ power law, while for longer times, a crossover to a weaker power law exponent is visible.
- The single-chain dynamic structure factor was measured by coherent NSE. As none of the conventional data evaluation schemes based solely on de Gennes' local reptation in combination with a lateral tube form factor yielded a good and comprehensive description, we used the novel Monkenbusch dynamic structure factor. We found that s-PP displays a strongly asymmetric tube with an aspect ratio of about 0.5. The fits improved, allowing for a small Non-Gaussianity of the Rouse blob dynamics.
- The tube dimension obtained from rheology is smaller than the effective tube diameter obtained from the dynamic pair-correlation function, with the corresponding ratio similar to that from other polymers, although C_∞ is considerably larger for s-PP.
- The scaling properties of the Monkenbusch dynamic structure factor are well fulfilled also for s-PP. Perfect scaling to PI that displays similar asymmetry is achieved. Finally, we note that counterintuitively the tube asymmetry appears not to be related to the chain stiffness, at least not in the range of C_∞ = 5 (PI) and 11.5 (s-PP).

■ ASSOCIATED CONTENT

Supporting Information

The Supporting Information is available free of charge at https://pubs.acs.org/doi/10.1021/acs.macromol.3c02529.

Sample characterization (absolute GPC) and additional fits of the dynamic structure factor (PDF)

■ AUTHOR INFORMATION

Corresponding Author

Michaela Zamponi − *Jülich Centre for Neutron Science at MLZ, Forschungszentrum Jülich GmbH, 85748 Garching, Germany;* orcid.org/0009-0007-2735-588X; Email: m.zamponi@fz-juelich.de

Authors

Wim Pyckhout-Hintzen − *Jülich Centre for Neutron Science (JCNS-1/IBI-8: Neutron Scattering and Biological Matter), Forschungszentrum Jülich GmbH, 52425 Jülich, Germany;* orcid.org/0000-0002-1142-359X

Andreas Wischnewski − *Jülich Centre for Neutron Science (JCNS-1/IBI-8: Neutron Scattering and Biological Matter), Forschungszentrum Jülich GmbH, 52425 Jülich, Germany*

Vitaliy Pipich − *Jülich Centre for Neutron Science at MLZ, Forschungszentrum Jülich GmbH, 85748 Garching, Germany;* orcid.org/0000-0002-3930-3602

Olaf Holderer − *Jülich Centre for Neutron Science at MLZ, Forschungszentrum Jülich GmbH, 85748 Garching, Germany;* orcid.org/0000-0001-6746-7965

Bela Farago − *Institut Laue-Langevin (ILL), F-38042 Grenoble, France*

https://doi.org/10.1021/acs.macromol.3c02529
Macromolecules 2024, 57, 3098−3108

Geoffrey W. Coates − *Department of Chemistry and Chemical Biology, Cornell University, Ithaca, New York 14853, United States;* orcid.org/0000-0002-3400-2552
Brian K. Long − *Department of Chemistry and Chemical Biology, Cornell University, Ithaca, New York 14853, United States*
Michael Monkenbusch − *Jülich Centre for Neutron Science (JCNS-1/IBI-8: Neutron Scattering and Biological Matter), Forschungszentrum Jülich GmbH, 52425 Jülich, Germany;* orcid.org/0000-0001-6733-832X
Dieter Richter − *Jülich Centre for Neutron Science (JCNS-1/IBI-8: Neutron Scattering and Biological Matter), Forschungszentrum Jülich GmbH, 52425 Jülich, Germany*

Complete contact information is available at: https://pubs.acs.org/10.1021/acs.macromol.3c02529

Notes

The authors declare no competing financial interest.

■ ACKNOWLEDGMENTS

The authors are thankful to J. den Doelder for providing the absolute GPC characterization. The authors acknowledge ILL for granting the beam time for the coherent NSE measurement.

■ REFERENCES

(1) Edwards, S. F. The statistical mechanics of polymerized material. *Proc. Phys. Soc.* **1967**, *92*, No. 9.
(2) de Gennes, P. G. Reptation of a polymer chain in the presence of fixed obstacles. *J. Chem. Phys.* **1971**, *55*, 572−579.
(3) Doi, M.; Edwards, S. F. *The Theory of Polymer Dynamics*; Clarendon Press: Oxford, 1988.
(4) Rouse, P. E. Theory of the linear viscoelastic properties of dilute solutions of coiling polymers. *J. Chem. Phys.* **1953**, *21*, 1272−1280.
(5) Wischnewski, A.; Monkenbusch, M.; Willner, L.; Richter, D.; Kali, G. Direct Observation of the Transition from Free to Constrained Single-Segment Motion in Entangled Polymer Melts. *Phys. Rev. Lett.* **2003**, *90*, No. 058302.
(6) Niedzwiedz, K.; Wischnewski, A.; Pyckhout-Hintzen, W.; Allgaier, J.; Richter, D.; Faraone, A. Chain Dynamics and Viscoelastic Properties of Poly(ethylene oxide). *Macromolecules* **2008**, *41*, 4866−4872.
(7) Monkenbusch, M.; Kruteva, M.; Richter, D. Dynamic structure factors of polymer melts as observed by neutron spin echo: Direct comparison and reevaluation. *J. Chem. Phys.* **2023**, *159*, No. 034902.
(8) Stephanou, P. S.; Baig, C.; Tsolou, G.; Mavrantzas, V. G.; Kröger, M. Quantifying chain reptation in entangled polymer melts: Topological and dynamical mapping of atomistic simulation results onto the tube model. *J. Chem. Phys.* **2010**, *132*, No. 124904.
(9) Rojo, E.; Muñoz, M. E.; Santamaría, A.; Peña, B. Correlation between Conformational Parameters and Rheological Properties of Molten Syndiotactic Polypropylenes. *Macromol. Rapid Commun.* **2004**, *25*, 1314−1318.
(10) Fetters, L. J.; Lohse, D. J.; Graessley, W. W. Chain Dimensions and Entanglement Spacings in Dense Macromolecular Systems. *J. Polym. Sci., Part B: Polym. Phys.* **1999**, *37*, 1023−1033.
(11) Tzounis, P.-N.; Argyropoulou, D. V.; Anogiannakis, S. D.; Theodorou, D. N. Tacticity Effect on the Conformational Properties of Polypropylene and Poly(ethylene−propylene) Copolymers. *Macromolecules* **2018**, *51*, 6878−6891.
(12) De Nicola, A.; Munaò, G.; Grizzuti, N.; Auriemma, F.; De Rosa, C.; Sevink, A.; Milano, G. Generation of well relaxed all atom models of stereoregular polymers: a validation of hybrid particle-field molecular dynamics for polypropylene melts of different tacticities. *Soft Mater.* **2020**, *18*, 228−241.
(13) de Gennes, P. G. Coherent scattering by one reptating chain. *J. Phys.* **1981**, *42*, 735−740.
(14) Richter, D.; Farago, B.; Butera, R.; Fetters, L. J.; Huang, J. S.; Ewen, B. On the origins of entanglement constraints. *Macromolecules* **1993**, *26*, 795−804.
(15) Wischnewski, A.; Monkenbusch, M.; Willner, L.; Richter, D.; Likhtman, A. E.; McLeish, T. C. B.; Farago, B. Molecular Observation of Contour-Length Fluctuations Limiting Topological Confinement in Polymer Melts. *Phys. Rev. Lett.* **2002**, *88*, No. 058301.
(16) Zamponi, M.; Kruteva, M.; Monkenbusch, M.; Willner, L.; Wischnewski, A.; Hoffmann, I.; Richter, D. Cooperative Chain Dynamics of Tracer Chains in Highly Entangled Polyethylene Melts. *Phys. Rev. Lett.* **2021**, *126*, No. 187801.
(17) Kruteva, M.; Zamponi, M.; Hoffmann, I.; Allgaier, J.; Monkenbusch, M.; Richter, D. Non-Gaussian and cooperative dynamics of entanglement strands in polymer melts. *Macromolecules* **2021**, *54*, 11384−11391.
(18) Guenza, M. G. Localization of Chain Dynamics in Entangled Polymer Melts. *Phys. Rev. E* **2014**, *89*, No. 052603.
(19) Akcasu, A. Z.; Tombakoglu, M. Dynamics of Copolymer and Homopolymer Mixtures in Bulk and in Solution via the Random Phase Approximation. *Macromolecules* **1990**, *23*, 607−612.
(20) Hammouda, B. SANS from homogeneous polymer mixtures: A unified overview. *Adv. Polym. Sci.* **1993**, *106*, 87−133.
(21) Likhtman, A. E.; McLeish, T. C. B. Quantitative theory for linear dynamics of linear entangled polymers. *Macromolecules* **2002**, *35*, 6332−6343.
(22) Baumgaertel, M.; Schausberger, A.; Winter, H. H. The relaxation of polymers with linear flexible chains of uniform length. *Rheol. Acta* **1990**, *29*, 400−408.
(23) Tian, J.; Hustad, P. D.; Coates, G. W. A new catalyst for highly syndiospecific living olefin polymerization: homopolymers and block copolymer from ethylene and propylene. *J. Am. Chem. Soc.* **2001**, *123*, 5134−5135.
(24) Holderer, O.; Monkenbusch, M.; Schätzler, R.; Kleines, H.; Westerhausen, W.; Richter, D. The JCNS neutron spin-echo spectrometer J-NSE at the FRM II. *Meas. Sci. Technol.* **2008**, *19*, No. 034022.
(25) Jones, T. D.; Chaffin, K. A.; Bates, F. S.; Annis, B. K.; Hagaman, E. W.; Kim, M.-H.; Wignall, G. D.; Fan, W.; Waymouth, R. Effect of Tacticity on Coil Dimensions and Thermodynamic Properties of Polypropylene. *Macromolecules* **2002**, *35*, 5061−5068.
(26) Witten, T. A.; Milner, S. T.; Wang, Z.-G. Theory of Stress Distribution in Block Copolymer Microdomains. In *Multiphase Macromolecular Systems*; Culbertson, B. M., Ed.; Plenum Press: New York, 1989.
(27) Fetters, L. J.; Lohse, D. J.; Richter, D.; Witten, T. A.; Zirkel, A. Connection between polymer molecular weight, density, chain dimensions, and melt viscoelastic properties. *Macromolecules* **1994**, *27*, 4639−4647.
(28) Eckstein, A.; Suhm, J.; Friedrich, C.; Maier, R.-D.; Sassmannshausen, J.; Bochmann, M.; Mülhaupt, R. Determination of Plateau Moduli and Entanglement Molecular Weights of Isotactic, Syndiotactic, and Atactic Polypropylenes Synthesized with Metallocene Catalysts. *Macromolecules* **1998**, *31*, 1335−1340.
(29) Liu, C.; Yu, J.; He, J.; Liu, W.; Sun, C.; Jing, Z. A Reexamination of G_N^0 and M_e of Syndiotactic Polypropylenes with Metallocene Catalysts. *Macromolecules* **2004**, *37*, 9279−9282.
(30) Monkenbusch, M.; Stadler, A.; Biehl, R.; Ollivier, J.; Zamponi, M.; Richter, D. Fast internal dynamics in alcohol dehydrogenase. *J. Chem. Phys.* **2015**, *143*, No. 075101.